AD-A192 930 TIME-DOMAIN BOUNDARY ELEMENT ANALYSIS OF DYNAMIC NEAR-TIP FIELDS FOR IMPA..(U) NORTHWESTERN UNIV EVANSTON IL STRUCTURAL MECHANICS LAB C ZHANG ET AL. 1/1

UNCLASSIFIED FEB 88 NU-SML-TR-88-1 N00014-85-K-0401 F/G 20/11 NL

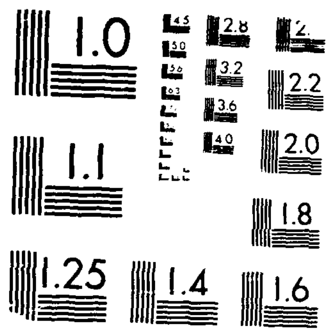

MICROCOPY RESOLUTION TEST CHART

STANDARDS 1963-A

TIME-DOMAIN BOUNDARY ELEMENT ANALYSIS OF DYNAMIC NEAR-TIP FIELDS FOR IMPACT-LOADED COLLINEAR CRACKS

Ch. Zhang and J. D. Achenbach

Center for Quality Engineering and Failure Prevention
Northwestern University
Evanston, IL 60208

Office of Naval Research

N00014-85-K-0401

February 1988

NU-SML-TR-88-1

Abstract

A time-domain boundary integral equation method has been developed to calculate elastodynamic fields generated by the incidence of stress (or displacement) pulses on single cracks and systems of two collinear cracks. The system of boundary integral equations has been cast in a form which is amenable to solution by the boundary element method in conjunction with a time-stepping technique. Particular attention has been devoted to dynamic overshoots of the stress intensity factors. Elastodynamic stress intensity factors for pulse incidence on a single crack have been computed as functions of time, and they have been compared with results of other authors. For collinear macrocrack-microcrack configurations the stress intensity factors at both tips of the macrocrack have been computed as functions of time for various values of the crack spacing and the relative size of the microcrack.

Introduction

The interaction of a stress pulse with a crack may give rise to dynamic overshoots of the stress intensity factors, i.e., larger stress intensity factors than would be obtained for quasi-static application of the external loads. For step-stress pulses the dynamic overshoot phenomenon has been noted by Achenbach [1], Thau and Lu [2] and Sih [3]. For the two dimensional configuration, Thau and Lu [2] used integral transform techniques in conjunction with a generalized Wiener-Hopf method to obtain exact but short-time dynamic stress intensity factors. Sih et al.[3] applied integral transform methods together with a numerical solution of dual integral equations and a numerical inversion of Laplace transforms to calculate dynamic stress-intensity factors. The problem has also been treated by finite-element [4] and finite difference methods [5]. An extension of the approach of Ref.[3] has been presented by Itou [6], who analyzed the fields for transient wave interaction with two coplanar cracks of equal length.

In this paper we investigate pulse-generated crack-tip fields by the use of a time-domain boundary integral equation (BIE) method. For wave interactions with volume scatterers, this technique has been successfully applied to two-dimensional elastodynamic problems by several authors, see, e.g., Niwa et al.[7], Manolis [8], Mansur [9], Antes [10],[11], and Estorff [12]. The usual displacement BIE formulation for scattering of elastic waves by volume scatterers degenerates, however, when the scatterer is reduced to a flat crack. A remedy for this difficulty is the use of "traction" BIE's, which results in a system of singular integral equations for the unknown crack opening displacements. Unfortunately, such BIE's are

highly singular and they cannot be solved directly by numerical methods. In the present paper this difficulty is overcome by reducing the higher order singularities to integrable singularities which can be integrated analytically or numerically. The simplified time-dependent BIE's are solved by the boundary element method in conjunction with a time-stepping technique. An alternative method has been proposed by Nishimura et al.[13] who used a double layer-regularization procedure. The numerical approach of the present paper has been applied to obtain time histories of elastodynamic stress intensity factors for single cracks as well as for configurations of a macrocrack and a collinear microcrack. Parametrical studies show the influence of the size and location of the microcrack on the effective stress intensity factors of the solitary crack.

The results for collinear cracks approximate the fields for macrocrack-microcrack configurations that are often observed in brittle materials such as ceramics, rocks and concretes. In such solids the high level of stress and deformation in the vicinity of a crack tip gives rise to microcracking and/or the formation of microvoids in a confined zone surrounding the macrocrack tip (see Bradt et al.[14], Carpinteri et al.[15], Hoagland et al.[16]). The existence of neighboring micro-cracks may significantly alter the stress intensity at the main crack tip, as shown by Kachanov et al.[17], Rubinstein [18] and Rose [19] for the static case. Depending on the size and location of microcracks or microvoids, their presence can either increase the stress intensity factors (stress amplification) or decrease it (stress shielding or toughening). Knowledge of the dependence of the stress intensity factors on the microdefects will assist in predicting macrocrack propagation. For static loading several studies can be found in the

literature, see Chen [20], Chudnovsky et al.[21],[22], Kachanov [23], Kachanov et al.[17], Rose [19], Rubinstein [18],[24] and Yokobori et al.[25].

Recently, Zhang and Achenbach [26],[27] have investigated the effects of microvoids and microcracks for time-harmonic wave loading. It was found that dynamic effects may give rise to considerable amplifications of the stress intensity factors.

2. Problem Statement

A two-dimensional configuration of a homogeneous, isotropic, linearly elastic body containing a macro-crack and a collinear neighboring micro-crack is shown in Fig. 1. An incident displacement pulse interacts with the two cracks, and generates a scattered displacement field. The propagation direction of the incident pulse is in the x_1x_2-plane, and the analysis of this paper is two-dimensional and for a state of plane strain. In terms of the incident field, $u_\alpha^{in}(\underset{\sim}{x},t)$, and the scattered field, $u_\alpha^{sc}(\underset{\sim}{x},t)$, the total displacement field may be written as

$$u_\alpha(\underset{\sim}{x},t) = u_\alpha^{in}(\underset{\sim}{x},t) + u_\alpha^{sc}(\underset{\sim}{x},t) \ , \quad \alpha = 1,2. \tag{2.1}$$

Similarly we have for the stress components

$$\sigma_{\alpha\beta}(\underset{\sim}{x},t) = \sigma_{\alpha\beta}^{in}(\underset{\sim}{x},t) + \sigma_{\alpha\beta}^{sc}(\underset{\sim}{x},t). \tag{2.2}$$

Since the faces of the cracks are free of tractions, the following conditions follow for the scattered field

$$\sigma^{sc}_{\alpha 2}(\underset{\sim}{x},t) = -\sigma^{in}_{\alpha 2}(\underset{\sim}{x},t) \quad \text{for} \quad \underset{\sim}{x} \in \Gamma_1 + \Gamma_2 \quad , \tag{2.3}$$

where Γ_1 and Γ_2 define the faces of the macro-crack and the micro-crack, respectively. The initial conditions are

$$u^{sc}_{\alpha}(\underset{\sim}{x},t) = \dot{u}^{sc}_{\alpha}(\underset{\sim}{x},t) \equiv 0 \quad \text{for } t < 0. \tag{2.4}$$

Here time t starts when the incident wave first reaches the crack.

The integral representation for the components of the scattered displacement field may be written as

$$u^{sc}_{\gamma}(\underset{\sim}{x}_p,t) = \int_o^t \int_{\Gamma_1+\Gamma_2} \sigma^{G}_{\alpha 2\gamma}(\underset{\sim}{x}_p,t;\underset{\sim}{x},\tau)\Delta u_{\alpha}\,(\underset{\sim}{x},\tau)dx_1 d\tau . \tag{2.5}$$

Here $\underset{\sim}{x}_p$ is the position vector of the observation point, $\sigma^{G}_{\alpha 2\gamma}$ is the stress Green's function for the uncracked plane (see Appendix A), and Δu_{α} is the displacement jump across the crack faces (the crack-opening displacement),

$$\Delta u_{\alpha}\,(x_1,0,\tau) = u_{\alpha}(x_1,0^+,\tau) - u_{\alpha}(x_1,0^-,\tau). \tag{2.6}$$

As shown in the next section, the solution to the problem formulated in this section can be reduced to the solution of a set of boundary integral equations.

3. Derivation of Discretized BIE's

In the conventional procedure BIE's can be derived from Eq.(2.5) by taking the limit $\underset{\sim}{x}_p \rightarrow \Gamma = \Gamma_1 + \Gamma_2$. However, such "displacement" BIE's degenerate for cracks, and hence they are not a valid basis for numerical modeling. This difficulty is overcome by the use of "traction" BIE's. These are obtained by substituting Eq.(2.5) into Hooke's law

$$\sigma_{\alpha\beta} = \lambda\delta_{\alpha\beta}u_{\gamma,\gamma} + \mu(u_{\alpha,\beta} + u_{\beta,\alpha}), \tag{3.1}$$

which yields a representation formula for the stress components $\sigma^{sc}_{\alpha 2}$ at the observation point $\underset{\sim}{x}_p$ as:

$$\sigma^{sc}_{\alpha 2}(\underset{\sim}{x}_p, t) = - \int_o^t \int_\Gamma K^G_{\alpha 2\delta\epsilon}(\underset{\sim}{x}_p, t; \underset{\sim}{x}, \tau)\Delta u_\delta(\underset{\sim}{x}, \tau) n_\epsilon ds d\tau, \quad \underset{\sim}{x}_p \notin \Gamma \quad , \tag{3.2}$$

where n_ϵ are the components of the normal vector to Γ, and

$$K^G_{\alpha\beta\delta\epsilon} = \lambda\delta_{\alpha\beta}\sigma^G_{\delta\epsilon\gamma,\gamma} + \mu(\sigma^G_{\delta\epsilon\alpha,\beta} + \sigma^G_{\delta\epsilon\beta,\alpha}) \quad . \tag{3.3}$$

Then, BIE's can be obtained from Eq.(3.2) by taking $\underset{\sim}{x}_p \rightarrow \Gamma$. Unfortunately, such "traction" BIE's are hyper singular when the observation point $\underset{\sim}{x}_p$ and the source point $\underset{\sim}{x}$ coincide, since in this case the kernel function $K^G_{\alpha\beta\delta\epsilon}$ of Eq.(3.2) behaves as

$$K^G_{\alpha\beta\delta\epsilon} \sim \frac{1}{r^2} \quad , \quad \text{if } r \rightarrow 0 \quad , \tag{3.4}$$

and

$$K^G_{\alpha\beta\delta\epsilon} \sim \frac{1}{\sqrt{[(t-\tau)^2-r^2/c^2_\alpha]^5}} \quad , \quad \text{if } (t-\tau)^2 \to r^2/c^2_\alpha \quad , \tag{3.5}$$

in which $r = |\underset{\sim}{x}-\underset{\sim}{x}_p|$, and c_α is either c_L or c_T, where

$$c^2_L = (\lambda+2\mu)/\rho \quad , \quad c^2_T = \mu/\rho. \tag{3.6}$$

A detailed discussion of these singularities can be found in a paper by Nishimura et al. [13].

To reduce these higher order singularities, Nishimura et al. [13] proposed a double layer-regularization procedure. In the present paper we apply another regularization method which has been developed by the authors in a recent paper [26] for scattering of incident time-harmonic elastic waves by multiple cracks.

Following the procedure of Zhang and Achenbach [26], we first divide Γ into J elements. Then Eq.(3.2) can be written in the following discretized form:

$$\sigma^{sc}_{\alpha 2}(\underset{\sim}{x}_p,t) = - \sum_{j=1}^{J} \int_o^t \int_{s_j}^{s_{j+1}} K^G_{\alpha 2\delta\epsilon}(\underset{\sim}{x}_p,t;\underset{\sim}{x},\tau)\Delta u_\delta(\underset{\sim}{x},\tau)n_\epsilon ds d\tau ,$$

$$\underset{\sim}{x}_p \notin \Gamma \quad , \tag{3.7}$$

where s_j and s_{j+1} are the endpoints of the j-th element. Because the main structure of the three terms in $K^G_{\alpha\beta\delta\epsilon}$ (see Eq.(3.3)) is similar, we will consider only the following integral

$$I_j = \int_{s_j}^{s_{j+1}} \sigma^G_{\delta\epsilon\gamma,\gamma} \Delta u_\delta n_\epsilon ds \quad . \tag{3.8}$$

By adding and subtracting the same terms, Eq.(3.8) can be rewritten as

$$I_j = \int_{s_j}^{s_{j+1}} (\sigma^G_{\delta\epsilon\gamma,\gamma} \Delta u_\delta n_\epsilon - \sigma^G_{\delta\epsilon\gamma,\epsilon} \Delta u_\delta n_\gamma) ds$$

$$+ \int_{s_j}^{s_{j+1}} \sigma^G_{\delta\epsilon\gamma,\epsilon} \Delta u_\delta n_\gamma ds \quad . \tag{3.9}$$

It can be shown that the first integral of (3.9) can be put into the following form (see Appendix B of Zhang and Achenbach [26])

$$\epsilon_{\gamma\epsilon} \sigma^G_{\epsilon\delta\gamma} \Delta u_\delta \Big|_{s_j}^{s_{j+1}} - \int_{s_j}^{s_{j+1}} \epsilon_{\gamma\epsilon} \epsilon_{\lambda\mu} \sigma^G_{\epsilon\delta\gamma} \Delta u_{\delta,\lambda} n_\mu ds \quad , \tag{3.10}$$

where $\epsilon_{\gamma\epsilon}$ denotes the two-dimensional permutation tensor. The second integral of Eq.(3.9) can be rewritten as

$$\int_{s_j}^{s_{j+1}} \sigma^G_{\delta\epsilon\gamma,\epsilon} \Delta u_\delta n_\gamma ds = \rho \int_{s_j}^{s_{j+1}} \ddot{u}^G_{\delta\gamma} \Delta u_\delta n_\gamma ds \quad , \tag{3.11}$$

where the equation of motion for the Green's function

$$\sigma^G_{\delta\epsilon\gamma,\epsilon} = \rho \ddot{u}^G_{\delta\gamma} \quad , \quad \underline{x}_P \neq \underline{x} \ , \quad t \neq \tau \quad , \tag{3.12}$$

has been used. Here $u^G_{\delta\gamma}$ is the Green's function for the displacement components (see Appendix A). Equation (3.10) and Eq. (3.11) together result in

$$I_j = \epsilon_{\gamma\epsilon}\sigma^G_{\epsilon\delta\gamma}\Delta u_\delta \Big|_{s_j}^{s_{j+1}} - \int_{s_j}^{s_{j+1}} \epsilon_{\gamma\epsilon}\epsilon_{\lambda\mu}\sigma^G_{\delta\epsilon\gamma}\Delta u_{\delta,\lambda}n_\mu ds$$

$$+ \rho \int_{s_j}^{s_{j+1}} \ddot{u}^G_{\delta\gamma}\Delta u_\delta n_\gamma ds \quad . \tag{3.13}$$

Using the same idea described above for the second and the third terms of Eq.(3.3) we obtain

$$\int_{s_j}^{s_{j+1}} K^G_{\alpha\beta\delta\epsilon}\Delta u_\delta n_\epsilon ds = H^1_{\alpha\beta\delta}\Delta u_\delta \Big|_{s_j}^{s_{j+1}} - \int_{s_j}^{s_{j+1}} H^1_{\alpha\beta\delta}\epsilon_{\lambda\mu}\Delta u_{\delta,\lambda}n_\mu ds$$

$$+ \rho \int_{s_j}^{s_{j+1}} H^2_{\alpha\beta\delta}\Delta u_\delta ds \quad , \tag{3.14}$$

where

$$H^1_{\alpha\beta\delta} = \lambda\delta_{\alpha\beta}\epsilon_{\gamma\epsilon}\sigma^G_{\delta\epsilon\gamma} + \mu(\epsilon_{\beta\epsilon}\sigma^G_{\delta\epsilon\alpha} + \epsilon_{\alpha\epsilon}\sigma^G_{\delta\epsilon\beta}) \quad , \tag{3.15}$$

$$H^2_{\alpha\beta\delta} = \lambda\delta_{\alpha\beta}u^G_{\delta\gamma}n_\gamma + \mu(u^G_{\delta\alpha}n_\beta + u^G_{\delta\beta}n_\alpha) \quad . \tag{3.16}$$

Furthermore, it can be shown that the following relation holds (Appendix B)

$$\int_o^t H^2_{\alpha\beta\delta}\Delta u_\delta d\tau = \int_o^t H^2_{\alpha\beta\delta}\Delta\ddot{u}_\delta d\tau \quad . \tag{3.17}$$

Substituting Eq.(3.14) and Eq.(3.17) into Eq.(3.7), taking the limit $\underset{\sim}{x}_p \to \Gamma$ and applying the boundary conditions on the cracks, Eq.(2.3), the following discretized BIE's are obtained

$$\sigma^{in}_{12}(\underset{\sim}{x}_p,t) = \sum_{j=1}^{J} \int_o^t \left\{ H^1_{121}\Delta u_1 \Big|_{s_j}^{s_{j+1}} - \int_{s_j}^{s_{j+1}} H^1_{121}\Delta u_{1,1} dx_1 + \rho \int_{s_j}^{s_{j+1}} H^2_{121}\Delta\ddot{u}_1 dx_1 \right\} d\tau \tag{3.18}$$

$$\sigma^{in}_{22}(\underset{\sim}{x}_p,t) = \sum_{j=1}^{J} \int_o^t \left\{ H^1_{222}\Delta u_2 \Big|_{s_j}^{s_{j+1}} - \int_{s_j}^{s_{j+1}} H^1_{222}\Delta u_{2,1} dx_1 + \rho \int_{s_j}^{s_{j+1}} H^2_{222}\Delta\ddot{u}_2 dx_1 \right\} d\tau \quad . \tag{3.19}$$

The integrals in (3.18) and (3.19) are to be understood in the sense of Cauchy principal values. It should be noted here that Eq.(3.18) and Eq.(3.19) are two decoupled BIE's for the unknown crack opening displacements Δu_1 and Δu_2 (as well as their derivatives). The singular terms of Eq.(3.18) and Eq.(3.19) at $\underset{\sim}{x}_p = \underset{\sim}{x}$ can be integrated analytically or numerically without difficulties as in the usual "displacement" BIE formulations. In the next section, we will present a time-stepping scheme for solving Eqs.(3.18) and (3.19).

4. Numerical Implementation

To solve the BIE's (3.18) and (3.19), discretization of time t is necessary. Here we have used equal time increments Δt, where $t_n = n\Delta t$ $(n = 1,2,\cdots N)$ denotes the time after the n-th time-step. The unknown crack opening displacements $\Delta u_\alpha(\underset{\sim}{x},\tau)$ in (3.18) and (3.19) are approximated by the following interpolation functions

$$\Delta u_\alpha(\underset{\sim}{x},\tau) = \sum_j \sum_n \mu_j(\underset{\sim}{x})\eta^n(\tau)(\Delta u_\alpha)_j^n \quad , \tag{4.1}$$

where $\mu_j(\underset{\sim}{x})$ and $\eta^n(\tau)$ have the properties

$$\mu_j(\underset{\sim}{x}^i) = \delta_{ij}, \quad \eta^n(\tau_m) = \delta_{mn} \quad , \tag{4.2}$$

In Eq.(4.2), $\underset{\sim}{x}^i$ defines the i-th nodal point, and

$$(\Delta u_\alpha)_i^m = \Delta u_\alpha(\underset{\sim}{x}^i,\tau_m) \tag{4.3}$$

represents the crack opening displacements at node i and at time $m\Delta t$.

In our analysis the function $\mu_j(\underset{\sim}{x})$ has been taken to be unity over each element except for elements near crack tips. For these elements a special shape function

$$\mu_j(\underset{\sim}{x}) = (a \mp x_1)^{\frac{1}{2}} \tag{4.4}$$

has been used to describe the proper behavior of Δu_α at the crack tips $x_1 = \pm a$. Higher order shape functions for $\eta^n(\tau)$ are desirable since Eqs.(3.18)

and (3.19) contain not only the functions Δu_α, but also their derivatives. In this paper the piecewise linear shape function

$$\eta^n(\tau) = \begin{cases} 1 - \dfrac{|\tau - n\Delta t|}{\Delta t} , & |\tau - n\Delta t| \le \Delta t , \\ 0 , & \text{otherwise} , \end{cases} \tag{4.5}$$

has been employed.

For each time-step Eqs.(3.18) and (3.19) can be rewritten as

$$\sigma_{12}^{in}(\underset{\sim}{x}_p, t_m) = \sum_{n=1}^{N} \sum_{j=1}^{J} \Bigg[L_{121}^{mn}(\underset{\sim}{x}_p;\underset{\sim}{x})\mu_j(\underset{\sim}{x}) \Bigg|_{s_j}^{s_{j+1}} - \int_{s_j}^{s_{j+1}} L_{121}^{mn}(\underset{\sim}{x}_p;\underset{\sim}{x}) \frac{\partial}{\partial x_1} \mu_j(\underset{\sim}{x}) dx_1 + \rho \int_{s_j}^{s_{j+1}} M_{121}^{mn}(\underset{\sim}{x}_p;\underset{\sim}{x})\mu_j(\underset{\sim}{x}) dx_1 \Bigg] (\Delta u_1)_j^n , \tag{4.6}$$

$$\sigma_{22}^{in}(\underset{\sim}{x}_p, t_m) = \sum_{n=1}^{N} \sum_{j=1}^{J} \Bigg[L_{222}^{mn}(\underset{\sim}{x}_p;\underset{\sim}{x})\mu_j(\underset{\sim}{x}) \Bigg|_{s_j}^{s_{j+1}} - \int_{s_j}^{s_{j+1}} L_{222}^{mn}(\underset{\sim}{x}_p;\underset{\sim}{x}) \frac{\partial}{\partial x_1} \mu_j(\underset{\sim}{x}) dx_1 + \rho \int_{s_j}^{s_{j+1}} M_{222}^{mn}(\underset{\sim}{x}_p;\underset{\sim}{x})\mu_j(\underset{\sim}{x}) dx_1 \Bigg] (\Delta u_2)_j^n . \tag{4.7}$$

In these equations the following abbreviations have been used

$$L^{mn}_{\alpha\beta\gamma}(\underset{\sim}{x}_p;\underset{\sim}{x}) = \int_{(n-1)\Delta t}^{(n+1)\Delta t} H^1_{\alpha\beta\gamma}(\underset{\sim}{x}_p,t_m;\underset{\sim}{x},\tau)\eta^n(\tau)d\tau, \tag{4.8}$$

$$M^{mn}_{\alpha\beta\gamma}(\underset{\sim}{x}_p;\underset{\sim}{x}) = \int_{(n-1)\Delta t}^{(n+1)\Delta t} H^2_{\alpha\beta\gamma}(\underset{\sim}{x}_p,t_m;\underset{\sim}{x},\tau)\eta^n(\tau)d\tau. \tag{4.9}$$

With Eq.(4.5), the time integrations in (4.8) and (4.9) can be performed analytically by using the integrals

$$\int_{(n-1)\Delta t}^{(n+1)\Delta t} \sigma^G_{\alpha\beta\gamma}(\underset{\sim}{x}_p,t_m;\underset{\sim}{x},\tau)\left[1 - \frac{|\tau-n\Delta t|}{\Delta t}\right] d\tau = S^L_{\alpha\beta\gamma} - S^T_{\alpha\beta\gamma} \quad , \tag{4.10}$$

and

$$\int_{(n-1)\Delta t}^{(n+1)\Delta t} H^2_{\alpha\beta\gamma}(\underset{\sim}{x}_p,t_m;\underset{\sim}{x},\tau)\eta^n(\tau)d\tau = \frac{1}{\Delta t}\{H^2_{\alpha\beta\gamma}[r,(m-n+1)\Delta t] - 2H^2_{\alpha\beta\gamma}[r,(m-n)\Delta t]$$

$$+ H^2_{\alpha\beta\gamma}[r,(m-n-1)\Delta t]\} \quad . \tag{4.11}$$

The functions $S^L_{\alpha\beta\gamma}$ and $S^T_{\alpha\beta\gamma}$ are given by

$$S^\xi_{\alpha\beta\gamma} = \frac{(c_T\Delta t)^2}{2\pi r^3}\left\{\frac{A_{\alpha\beta\gamma}}{3}\left[D^{\xi 3}_{mn}(r,1) - 2D^{\xi 3}_{mn}(r,0) + D^{\xi 3}_{mn}(r,-1)\right] -\right.$$

$$\left. - B^\xi_{\alpha\beta\gamma}\left(\frac{r}{c_\xi\Delta t}\right)^2\left[D^{\xi 1}_{mn}(r,1) - 2D^{\xi 1}_{mn}(r,0) + D^{\xi 1}_{mn}(r,-1)\right]\right\} \quad ,$$

$$\xi = L,T, \tag{4.12}$$

where $A_{\alpha\beta\gamma}$, $B^L_{\alpha\beta\gamma}$ and $B^T_{\alpha\beta\gamma}$ can be found in Appendix A, and the function

$D^{\xi p}_{mn}(r,q)$ is defined as

$$D^{\xi p}_{mn}(r,q) = \begin{cases} [(m-n-q)^2 - r^2/(c_\xi \Delta t)^2]^{p/2} \;, & \text{if } (m-n-q) > r/(c_\xi \Delta t), \\ 0 \;, & \text{otherwise.} \end{cases} \tag{4.13}$$

By choosing J collocation points on Γ and N points for t, and requiring that Eqs.(4.6) and (4.7) are satisfied at each discrete point $\underset{\sim}{x}^i_P$ $(i = 1,2,\cdots J)$, we obtain a system of linear algebraic equations which must be solved at each time $t_m = m\Delta t$ $(m = 1,2,\cdots N)$:

$$f^m_i = \sum_{n=1}^{N} \sum_{j=1}^{J} A^{mn}_{ij} (\Delta u_1)^n_j \quad , \tag{4.14}$$

$$g^m_i = \sum_{n=1}^{N} \sum_{j=1}^{J} B^{mn}_{ij} (\Delta u_2)^n_j \quad , \tag{4.15}$$

where

$$f^m_i = \sigma^{in}_{12}(\underset{\sim}{x}^i_P, t_m) \quad , \tag{4.16}$$

$$g^m_i = \sigma^{in}_{22}(\underset{\sim}{x}^i_P, t_m) \quad , \tag{4.17}$$

$$A^{mn}_{ij} = L^{mn}_{121}(\underset{\sim}{x}^i_P;\underset{\sim}{x})\mu_j(\underset{\sim}{x}) \Big|^{s_{j+1}}_{s_j} - \int_{s_j}^{s_{j+1}} L^{mn}_{121}(\underset{\sim}{x}^i_P;\underset{\sim}{x}) \frac{\partial}{\partial x_1} \mu_j(\underset{\sim}{x}) dx_1$$

$$+ \rho \int_{s_j}^{s_{j+1}} M^{mn}_{121}(\underset{\sim}{x}^i_P;\underset{\sim}{x})\mu_j(\underset{\sim}{x}) dx_1 \quad , \tag{4.18}$$

$$B_{ij}^{mn} = L_{222}^{mn}(\underset{\sim}{x}_P^i;\underset{\sim}{x})\mu_j(\underset{\sim}{x}) \Big|_{s_j}^{s_{j+1}} - \int_{s_j}^{s_{j+1}} L_{222}^{mn}(\underset{\sim}{x}_P^i;\underset{\sim}{x})\frac{\partial}{\partial x_1} \mu_j(\underset{\sim}{x})dx_1$$

$$+ \rho \int_{s_j}^{s_{j+1}} M_{222}^{mn}(\underset{\sim}{x}_P^i;\underset{\sim}{x}) \; \mu_j(\underset{\sim}{x})dx_1 \; . \qquad (4.19)$$

Here we will discuss only A_{ij}^{mn} in some more detail, since the main structure of A_{ij}^{mn} and B_{ij}^{mn} is the same. At first sight it seems that N^2J^2 discrete kernels A_{ij}^{mn} have to be calculated. However, this number can be reduced to NJ^2, if we use the causality properties

$$u_{\alpha\gamma}^G(\underset{\sim}{x}_P,t_m;\underset{\sim}{x},t_n) = 0 \quad , \quad \text{if } n > m \quad , \qquad (4.20)$$

$$\sigma_{\alpha\beta\gamma}^G(\underset{\sim}{x}_P,t_m;\underset{\sim}{x},t_n) = 0 \quad , \quad \text{if } n > m \quad , \qquad (4.21)$$

and the following time translation properties of the Green's functions (Appendix A):

$$u_{\alpha\gamma}^G(\underset{\sim}{x}_P,t_m;\underset{\sim}{x},t_n) = u_{\delta\gamma}^G(\underset{\sim}{x}_P,t_m+ t_\ell;\underset{\sim}{x},t_n + t_\ell) \quad , \qquad (4.22)$$

$$\sigma_{\alpha\beta\gamma}^G(\underset{\sim}{x}_P,t_m;\underset{\sim}{x},t_n) = \sigma_{\delta\beta\gamma}^G(\underset{\sim}{x}_P,t_m+ t_\ell;\underset{\sim}{x},t_n + t_\ell) \quad , \qquad (4.23)$$

Thus, the matrix A_{ij}^{mn} has the following special form

$$\begin{bmatrix} A_{ij}^{11} & & & 0 \\ A_{ij}^{21} & A_{ij}^{22} & & \\ A_{ij}^{31} & A_{ij}^{32} & A_{ij}^{33} & \\ \vdots & \vdots & \vdots & \ddots \\ A_{ij}^{m1} & A_{ij}^{m2} & \cdots & A_{ij}^{mm} \end{bmatrix} = \begin{bmatrix} A_{ij}^{1} & & & 0 \\ A_{ij}^{2} & A_{ij}^{1} & & \\ A_{ij}^{3} & A_{ij}^{2} & A_{ij}^{1} & \\ \vdots & \vdots & \vdots & \ddots \\ A_{ij}^{q} & A_{ij}^{q-1} & \cdots & A_{ij}^{1} \end{bmatrix} \tag{4.24}$$

where q is defined by

$$q = m-n+1 \quad . \tag{4.25}$$

The form of B_{ij}^{mn} is similar to A_{ij}^{mn}, and it will not be given here for brevity.

By considering this special structure of A_{ij}^{mn} and B_{ij}^{mn} we obtain finally the following time-stepping scheme:

$$\begin{cases} (\Delta u_1)_i^1 = \sum_{j=1}^{J} (A_{ij}^1)^{-1} f_j^1 \quad , \\ (\Delta u_1)_i^q = \sum_{j=1}^{J} (A_{ij}^1)^{-1} [f_j^q - \sum_{p=1}^{q-1} A_{jk}^{(q-p+1)} (\Delta u_1)_k^p] \quad , \end{cases} \tag{4.26a,b}$$

$$\begin{cases} (\Delta u_2)_i^1 = \sum_{j=1}^{J} (B_{ij}^1)^{-1} g_j^1 \quad , \\ (\Delta u_2)_i^q = \sum_{j=1}^{J} (B_{ij}^1)^{-1} \left[g_j^q - \sum_{p=1}^{q-1} B_{jk}^{(q-p+1)} (\Delta u_2)_k^p\right] \quad , \end{cases} \tag{4.27a,b}$$

in which $(A^1_{ij})^{-1}$ and $(B^1_{ij})^{-1}$ denote the elements of the inverse matrix of $\underline{A}^1$ and $\underline{B}^1$ at the first time step. Also, $q = 2,3,\cdots N$.

At each time step only one blockmatrix A^q_{ij} (and B^q_{ij}) has to be evaluated. For the first time step, the inverse matrix $(\underline{A}^1)^{-1}$ and $(\underline{B}^1)^{-1}$ must also be determined. Spatial integrations in Eq.(4.18) and Eq.(4.19) have been performed analytically for the constant shape function ($\mu_j(\underline{x}) = 1$), and numerically for the "crack-tip" shape function (see Eq.(4.4)) by using an 8-points Gauss-Jacobian formula. In the latter case, the singular terms have been integrated analytically and numerically.

5. Dynamic Stress Intensity Factors

Once the crack opening displacements, Δu_δ, have been calculated from the time-stepping scheme as described in the last section, stress intensity factors can be calculated by using the following well-known relations [30]

$$\begin{Bmatrix} K^{\pm}_I(t) \\ K^{\pm}_{II}(t) \end{Bmatrix} = \frac{\mu\sqrt{2\pi}}{4(1-\nu)} \lim_{x_1 \to \pm a} \frac{1}{(a \mp x_1)^{1/2}} \begin{Bmatrix} \Delta u_2(x_1,t) \\ \Delta u_1(x_1,t) \end{Bmatrix} , \qquad (5.1)$$

where "+" indicates the tip at $x_1 = a$ and "-" indicates the tip at $x_1 = -a$, while ν denotes Poisson's ratio.

In the numerical calculations, the incident wave was taken as either a plane longitudinal wave of the form

$$u^{in}_\alpha = U_L \begin{Bmatrix} \sin\phi \\ \cos\phi \end{Bmatrix} [c_L t - (x_1+a)\sin\phi - x_2\cos\phi] \cdot H[c_L t - (x_1+a)\sin\phi - x_2\cos\phi] \qquad (5.2)$$

or a plane transverse wave of the form

$$u_\alpha^{in} = U_T \begin{Bmatrix} -\cos\phi \\ \sin\phi \end{Bmatrix} [c_T t - (x_1+a)\sin\phi - x_2\cos\phi] \cdot H[c_T t - (x_1+a)\sin\phi - x_2\cos\phi], \quad (5.3)$$

where U_L and U_T are the displacement amplitudes, ϕ is the angle of incidence, and $H(\cdot)$ is the Heaviside function. The corresponding stress components are

$$\sigma_{11}^{in} = U_L(\lambda+2\mu - 2\mu\cos^2\phi)H[c_L t-(x_1+a)\sin\phi - x_2\cos\phi], \quad (5.4)$$

$$\sigma_{12}^{in} = U_L\mu\sin(2\phi)H[c_L t-(x_1+a)\sin\phi - x_2\cos\phi], \quad (5.5)$$

$$\sigma_{22}^{in} = U_L(\lambda+2\mu - 2\mu\sin^2\phi)H[c_L t-(x_1+a)\sin\phi - x_2\cos\phi], \quad (5.6)$$

for an incident longitudinal wave, and

$$\sigma_{11}^{in} = -U_T\mu\sin(2\phi)H[c_T t-(x_1+a)\sin\phi - x_2\cos\phi], \quad (5.7)$$

$$\sigma_{12}^{in} = - U_T\mu\cos(2\phi)H[c_T t-(x_1+a)\sin\phi - x_2\cos\phi], \quad (5.8)$$

$$\sigma_{22}^{in} = U_T\mu\sin(2\phi)H[c_T t-(x_1+a)\sin\phi - x_2\cos\phi] \quad (5.9)$$

for an incident transverse wave.

All calculations have been carried out for a Poisson's ratio $\nu = 1/4$. The geometrical configuration is shown in Fig. 1. The principal (macro) crack has been discretized into 50 elements of equal length, and a proportional number of elements have been used for the micro-crack.

For $b/a = 0$, the configuration reduces to a single crack of length 2a. This case was used to check numerical results obtained by our method. Comparisons with Thau and Lu's results [2] are given in Figures 2a and 2b. Figure 2a presents results for normal incidence of a longitudinal (L) wave, while Fig. 2b is for a normally incident transverse (TV) wave. All results are normalized by the corresponding static values. The agreements are very good, especially in the overall variation of the stress intensity factors with time and in their peak values. Calculations for inclined incidence ($\phi \neq 0$) of L or TV waves have also been carried out, and the agreements with Thau and Lu's results are again very good. The time increment was selected as $c_T \Delta t = 0.08a$. The influence of Δt on the stability of the time-stepping scheme has been studied numerically, and it was found that too small a value of Δt may cause instabilities for the results at large time. The same conclusions have been drawn by Nishimura et al.[13]. The time increment chosen here always yielded good results, and hence, this value has also been used for the macro-microcrack interaction problems.

For a fixed half-length of the microcrack, $b/a = 0.1$, and for normal incidence of a longitudinal wave ($\phi = 0^o$), the dynamic stress intensity factors are shown in Figures 3a,b, versus the dimensionless time $c_L t/a$, for various values of the crack-tip distance d/a. All results have been normalized by the static stress intensity factors of a single crack under the corresponding static load. Due to symmetry with respect to $x_2 = 0$, the Mode-II stress intensity factors are identically zero, $\bar{K}_{II}^{\pm} \equiv 0$. Figure 3a shows that, as expected, the presence of a microcrack does not influence the left tip of the macrocrack at small time. However, after $c_L t/a \simeq 3$ the difference between both cases becomes somewhat distinct. It is, however,

evident that the crack-tip away from the microcrack is not significantly affected by the presence of a collinear microcrack. The presence of a microcrack, does, however, give rise to a substantial increase of the stress intensity factor at the tip adjoining the microcrack (Fig. 3b). The $\overline{K}_I^+$-factor increases with decreasing crack-tip distance d/a, and considerable amplifications in $\overline{K}_I^+$ occur for very small values of d/a. At both tips of the main crack, the maximum dynamic stress intensity factors exceed the corresponding static values, which are reached at large time t. Both $\overline{K}_I^+$ and $\overline{K}_I^-$, assume the values for a single solitary crack of half-length a as $d/a \to \infty$.

Figures 4a,b and Figures 5a,b show the normalized dynamic stress intensity factors when a longitudinal wave is indcident under an angle $\phi = 30°$. Both the $\overline{K}_I^{\pm}$ and $\overline{K}_{II}^{\pm}$ factors are present in this case. The time history of $\overline{K}_I^-$ (Fig. 4a) is very similar to that for normal incidence (Fig. 3a). The $\overline{K}_I^+$-factor at the tip adjoining the microcrack, which is zero before the incident wave front arrives at this tip ($c_L t/a < 1$), is shown in Fig. 4b. The smaller the distance between microcrack and main crack, the larger is the stress intensity at the crack-tip adjoining the microcrack. It is also interesting that the maximums of the normalized values $\overline{K}_I^{\pm}$ are the same as those for normal incidence. Results for $\overline{K}_{II}^{\pm}$ are given in Figures 5a,b. Their variations with the dimensionless time $c_L t/a$, and their dependence on the crack-tip distance d/a, are similar to those of the $\overline{K}_I^{\pm}$-factors. The overshoots of the Mode-II dynamic stress intensity factors are, however, less than those of the Mode-I cases.

It is evident that the dynamic stress intensity factors depend strongly on both the location and the size of the microcrack. For a fixed crack-tip distance, $d/a = 0.05$, and for normal incidence of a longitudinal wave ($\phi = 0^o$), the dependence of the $\bar{K}_I^{\pm}$-factors on the dimensionless half-length of the microcrack, b/a, is shown in Figures 6a,b. As before, at small time, the crack-tip away from the microcrack behaves as the tip of a semi-infinite crack, and $\bar{K}_I^-$ is the same for all five cases (proportional to $\sqrt{c_L t/a}$). The influence of the microcrack (as well as the crack-tip adjoining the microcrack) on $\bar{K}_I^-$ becomes important when diffracted waves arrive at the left tip of the main crack. The peak $\bar{K}_I^-$-factor increases with increasing b/a, but it is shifted to somewhat larger time $c_L t/a$. The $\bar{K}_I^-$-factor for larger b/a can be slightly smaller than for a shorter microcrack (smaller b/a), which is in contrast to the static case (see Yokobori et al.[25]). Figure 6b shows the variation of $\bar{K}_I^+$ with the microcrack size b/a. As expected, a larger microcrack gives rise to a larger amplification of the stress intensity factors. For $b/a = 0$ the configuration reduces to a single crack, and in this case we have $\bar{K}_I^+ = \bar{K}_I^-$.

Acknowledgment

The work reported here was carried out in the course of research sponsored by the Office of Naval Reseach under Contract N00014-85-K-0401 with Northwestern University. A Grant from Cray Research Inc. for access to the Pittsburgh Supercomputer Center is also gratefully acknowledged.

References

[1] J.D. Achenbach, Dynamic Effects in Brittle Fracture, in Mechanics Today, 1, pp. 1-57. Pergamon, New York (1972).

[2] S.A. Thau and T.H. Lu, Transient Stress Intensity Factors for a Finite Crack in an Elastic Solid Caused by a Dilatational Wave, Int. J. Solids Structures, 7, 731-750 (1971).

[3] G.C. Sih, G.T. Embley, and R.S. Ravera, Impact Response of a Finite Crack in Plane Extension, Int. J. Solids Structures, 8, 977-993 (1972).

[4] S.N. Atluri, and T. Nishioka, Numerical Studies in Dynamic Fracture Mechanics, Int. J. Fracture, 27, 646-651 (1985).

[5] A. Peuser, Ein Beitrag zur Analyse stationärer und instationärer dynamischer Rißprobleme, Dissertation, TH Darmstadt (1983).

[6] S. Itou, Transient Analysis of Stress Waves Around Two Coplanar Griffith Cracks Under Impact Load, Eng. Fract. Mech., 13, 349-356 (1980).

[7] Y. Niwa, T. Fukui, S. Kato and K. Fuji, An Application of the Integral Equation Method for Two-Dimensional Elastodynamics, Theor. Appl. Mech., 28, 281-290 (1980).

[8] G. Manolis, A Comparative Study on Three Boundary Element Method Approaches to Problems in Elastodynamics, Int. J. Numer. Meths. Engng., 19, 73-91 (1983).

[9] W.J. Mansur, A Time-Stepping Technique to Solve Wave Propagation Problems Using the Boundary Element Method, Ph.D. Thesis, Univ. of Southampton (1983).

[10] H. Antes, A Boundary Element Procedure for Transient Wave Propagations in Two-Dimensional Isotropic Elastic Media, Finite Elements in Analysis and Design, 1, 313-322 (1985).

[11] H. Antes, Anwendung der Randelementmethode in der Elasto- und Fluiddynamik, Teubner-Verlag (1987).

[12] O.v. Estorff, Zur Berechnung der dynamischen Wechselwirkung zwischen Bauwerken und ihrer Umgebung mittels zeitabhängiger Randintegralgleichungen, Report TWM 86-10, Inst. f. Konstr. Ingenieurbau, Ruhr-Universität Bochum (1986).

[13] N. Nishimura, Q.C. Guo and S. Kobayashi, Boundary Integral Equation Methods in Elastodynamic Crack Problems, Proc. 9th Int. Conf. BEM, Vol 2 (Eds. W.L. Wendland and C.A. Brebbia), Springer-Verlag, pp. 279-291 (1987).

[14] R. Bradt, D. Hasselman and F. Lange (Editors), Fracture Mechanics of Ceramics, 2, Plenum Press, New York (1974).

[15] A. Carpinteri and A. Ingraffea (Editors), Fracture Mechanics of Concrete, Nijhoff (1984).

[16] R. Hoagland, G. Hahn and A. Rosenfield, Influence of Microstructure on the Fracture Propagation in Rock, Rock Mech., 5, 77-106 (1973).

[17] M. Kachanov and E. Montagut. Interaction of a Crack with Certain Microcrack Arrays, Eng. Fract. Mech., 25, 625-636 (1986).

[18] A.A. Rubinstein, Macrocrack-Microdefect Interaction, ASME J. Appl. Mech., 53, 505-510 (1986).

[19] L.R.F. Rose, Microcrack Interaction with a Main Crack, Int. J. Fracture, 31, 233-242 (1986).

[20] Y.H. Chen, Effect of a Hole near a Crack Tip on the Stress Intensity Factor, Int. J. Fracture, 32, R39-R42 (1987).

[21] A. Chudnovsky and M. Kachanov, Interaction of a Crack with a Field of Microcracks, Int. J. Engng. Sci., 21, 1009-1018 (1983).

[22] A. Chudnovsky, A. Dolgopolsky and M. Kachanov, Elastic Interaction of a Crack with Microcracks, in: Advances in Fracture Research, Proc. Sixth Conf. on Fracture, New Dehli, India, 2, 825-833 (1984).

[23] M. Kachanov, A Simple Technique of Stress Analysis in Elastic Solids with Many Cracks, Int. J. Fracture, 28, R11-R19 (1985).

[24] A.A. Rubinstein, Macrocrack Interaction with Semi-Infinite Microcrack Array, Int. J. Fracture, 27, 113-119 (1985).

[25] T. Yokobori, M. Ohashi and M. Ichikawa, The Interaction of two Collinear Asymmetric Elastic Cracks, Reports of the Research Institute for Strength and Fracture of Materials, Tohoku University, 1, 33-39 (1965).

[26] Ch. Zhang and J.D. Achenbach, Scattering by Multiple Cracks, J. Appl. Mech., in press.

[27] Ch. Zhang and J.D. Achenbach, Effect of an Adjacent Cavity on the Interaction of Elastic Waves with a Crack, submitted for publication.

[28] J.D. Achenbach, Wave Propagation in Elastic Solids, North-Holland (1973).

[29] A.C. Eringen and E.S. Suhubi, Elastodynamics II, Academic Press, New York, San Francisco, London (1975)

[30] F. Erdogan, Stress Intensity Factors, ASME J. Appl. Mech., 50, 992-1002(1983).

Appendix A

The Green's Function

The two-dimensional elastodynamic Green's function is given by (see [28], [29])

$$u^G_{\alpha\gamma}(\underset{\sim}{x}_P,t;\underset{\sim}{x},\tau) = \frac{1}{2\pi\rho}\left\{\frac{1}{c_L r^2} H[c_L(t-\tau)-r]\left[\frac{2c_L^2(t-\tau)^2-r^2}{R_L} r,_\alpha r,_\gamma\right.\right.$$

$$\left. - R_L\delta_{\alpha\gamma}\right] - \frac{1}{c_T r^2} H[c_T(t-\tau)-r]\left[\frac{2c_T^2(t-\tau)^2-r^2}{R_T} r,_\alpha r,_\gamma -\right.$$

$$\left.\left. - \frac{c_T^2(t-\tau)^2}{R_T}\delta_{\alpha\gamma}\right]\right\} \quad , \qquad (A.1)$$

where

$$r = |\underset{\sim}{x}-\underset{\sim}{x}_P| \quad , \quad R_\xi = \sqrt{c_\xi^2(t-\tau)^2-r^2}, \quad \xi = L,T \quad , \qquad (A.2)$$

and $H(\cdot)$ is the Heaviside step function. The function $u^G_{\alpha\gamma}(\underset{\sim}{x}_P,t;\underset{\sim}{x},\tau)$ denotes the displacement in the α-direction observed at position $\underset{\sim}{x}$ and at time t, due to a unit force in the γ direction, applied at position $\underset{\sim}{x}_P$ and at time τ. The corresponding stress components follow from (A.1) and Hooke's law as

$$\sigma^G_{\alpha\beta\gamma}(\underset{\sim}{x}_P,t;\underset{\sim}{x},\tau) = \frac{1}{2\pi r^3}\left\{\frac{1}{\kappa} H[c_L(t-\tau)-r]\left[\frac{2c_L^2(t-\tau)^2-r^2}{R_L} A_{\alpha\beta\gamma} +\right.\right.$$

$$\left. + \frac{r^4}{R_L^3} B^L_{\alpha\beta\gamma}\right] - H[c_T(t-\tau)-r]\left[\frac{2c_T^2(t-\tau)^2-r^2}{R_T} A_{\alpha\beta\gamma} +\right.$$

$$+ \quad \frac{r^4}{R_T^5} B^T_{\alpha\beta\gamma} \Big] \Big\} \quad , \tag{A.3}$$

in which

$$A_{\alpha\beta\gamma} = 2(\delta_{\alpha\beta} r,_{\gamma} + \delta_{\beta\gamma} r,_{\alpha} + \delta_{\alpha\gamma} r,_{\beta} - 4r,_{\alpha} r,_{\beta} r,_{\gamma}) \quad , \tag{A.4}$$

$$B^L_{\alpha\beta\gamma} = (\kappa^2 - 2)\delta_{\alpha\beta} r,_{\gamma} + 2r,_{\alpha} r,_{\beta} r,_{\gamma} \quad , \tag{A.5}$$

$$B^T_{\alpha\beta\gamma} = 2r,_{\alpha} r,_{\beta} r,_{\gamma} - \delta_{\alpha\gamma} r,_{\beta} - \delta_{\beta\gamma} r,_{\alpha} \quad , \tag{A.6}$$

$$\kappa = c_L / c_T \quad . \tag{A.7}$$

The function $u^G_{\alpha\gamma}(\underset{\sim}{x}_P, t; \underset{\sim}{x}, \tau)$ has the following properties

1) causality

$$u^G_{\alpha\gamma}(\underset{\sim}{x}_P, t; \underset{\sim}{x}, \tau) = 0 \quad , \quad \text{if } c_L(t-\tau) < |\underset{\sim}{x} - \underset{\sim}{x}_P| \quad , \tag{A.8}$$

2) time translation

$$u^G_{\alpha\gamma}(\underset{\sim}{x}_P, t+t_\ell; \underset{\sim}{x}, t+t_\ell) = u^G_{\alpha\gamma}(\underset{\sim}{x}_P, t; \underset{\sim}{x}, \tau) \quad . \tag{A.9}$$

The functions $\partial u^G_{\alpha\gamma}/\partial\tau$ and $\sigma^G_{\alpha\beta\gamma}$ also possess these causality and time translation properties.

Appendix B

Proof of Eq.(3.17)

To prove the identity, Eq.(3.17), it is sufficient to consider only the first term of $H^2_{\alpha\beta\delta}$ since the three terms of $H^2_{\alpha\beta\delta}$ have similar forms. We consider

$$\int_0^t \ddot{u}^G_{\delta\gamma}\Delta u_\delta d\tau = \lim_{\epsilon\to 0^+} \int_0^{t+\epsilon} \ddot{u}^G_{\delta\gamma}\Delta u_\delta d\tau \ . \tag{B.1}$$

Partial integration of the right hand side of (B.1) yields

$$\lim_{\epsilon\to 0^+} \int_0^{t+\epsilon} \ddot{u}^G_{\delta\gamma}\Delta u_\delta d\tau = \lim_{\epsilon\to 0^+} \left[\dot{u}^G_{\delta\gamma}\Delta u_\delta d\tau \Big|_0^{t+\epsilon} - \int_0^{t+\epsilon} \dot{u}^G_{\delta\gamma}\Delta\dot{u}_\delta d\tau \right]$$

$$= \lim_{\epsilon\to 0^+} \left[\dot{u}^G_{\delta\gamma}\Delta u_\delta d\tau \Big|_0^{t+\epsilon} - u^G_{\delta\gamma}\Delta\dot{u}_\delta \Big|_0^{t+\epsilon} + \int_0^{t+\epsilon} u^G_{\delta\gamma}\Delta\ddot{u}_\delta d\tau \right] , \tag{B.2}$$

The first two terms in (B.2) vanish due to the initial conditions on Δu_δ and $\Delta \dot{u}_\delta$, and due to the causality properties of $u^G_{\delta\gamma}$ and $\dot{u}^G_{\delta\gamma}$. Thus, we obtain

$$\int_0^t \ddot{u}^G_{\delta\gamma}\Delta u_\delta d\tau = \int_0^t u^G_{\delta\gamma}\Delta\ddot{u}_\delta d\tau \ . \tag{B.3}$$

Equation (3.17) can be derived directly from (3.16) and (B.3).

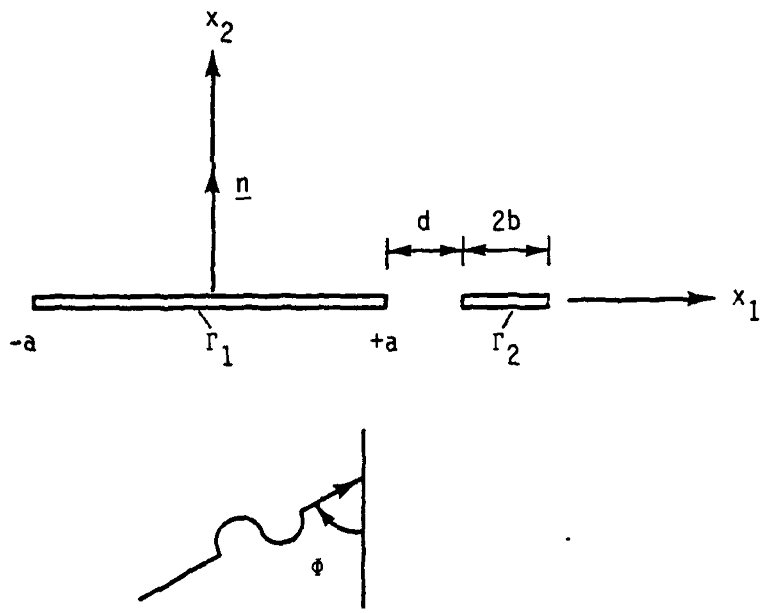

Fig. 1: Macrocrack-microcrack configuration.

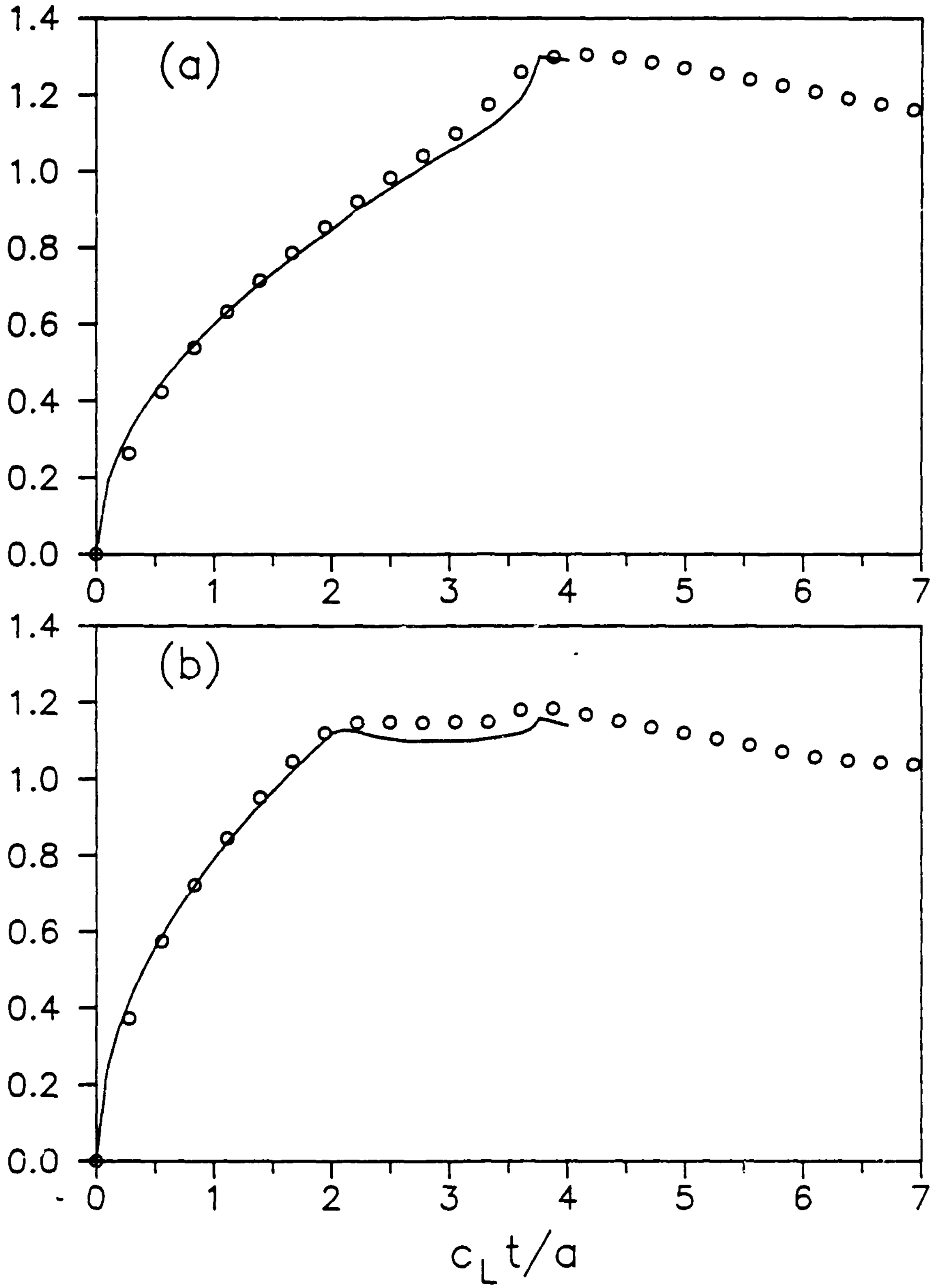

Fig. 2: Normalized dynamic stress intensity factors for a single crack, and for normal incidence of a plane wave, —— Thau and Lu, o o o present work; (a) $\overline{K}_I^{\pm}$ for L-wave incidence; (b) $\overline{K}_{II}^{\pm}$ for TV-wave incidence.

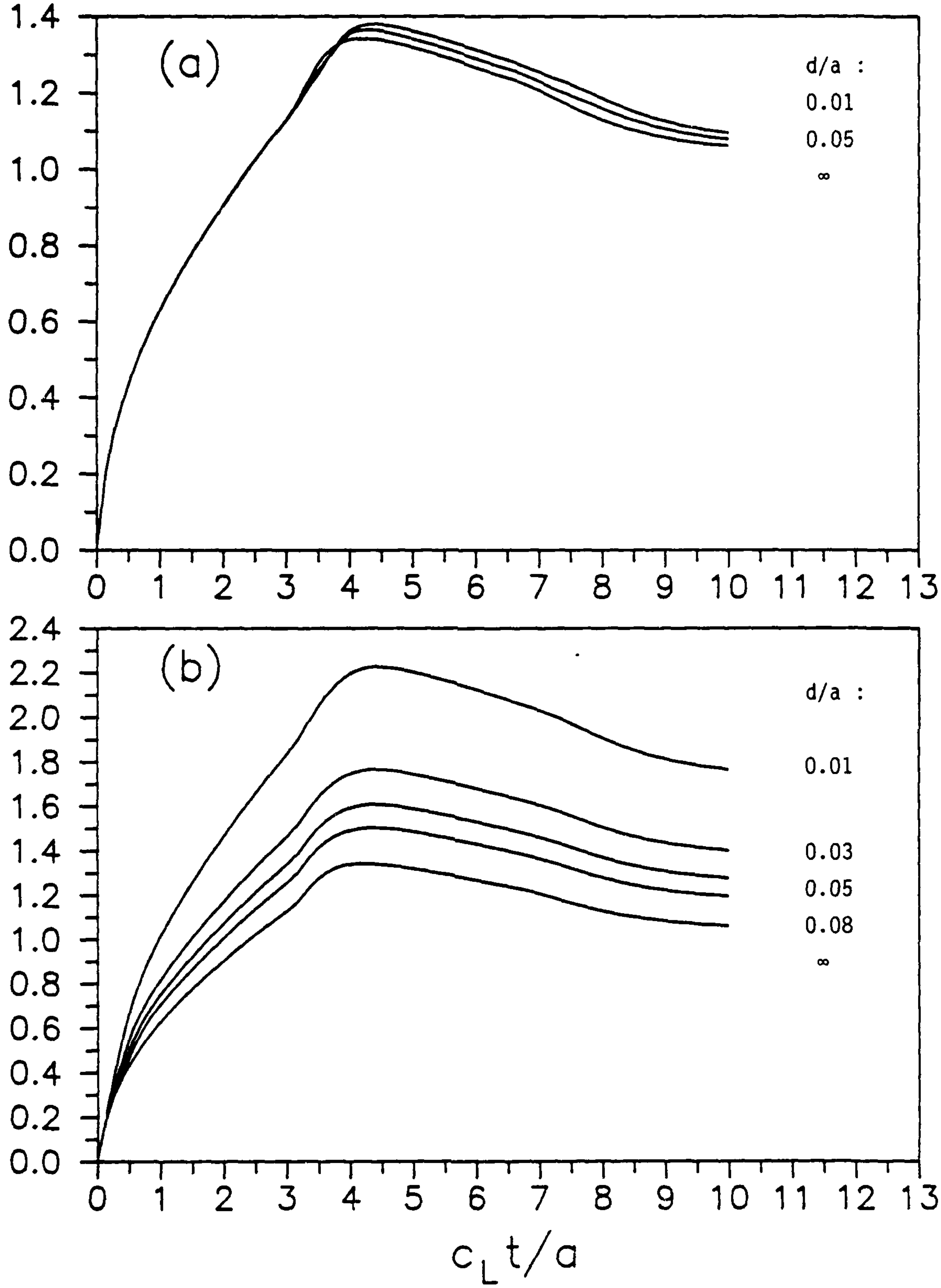

Fig. 3: Normalized stress intensity factors for various d/a, and for normal incidence of a plane L-wave, b/a = 0.1; (a) $\overline{K_I^-}$; (b) $\overline{K_I^+}$.

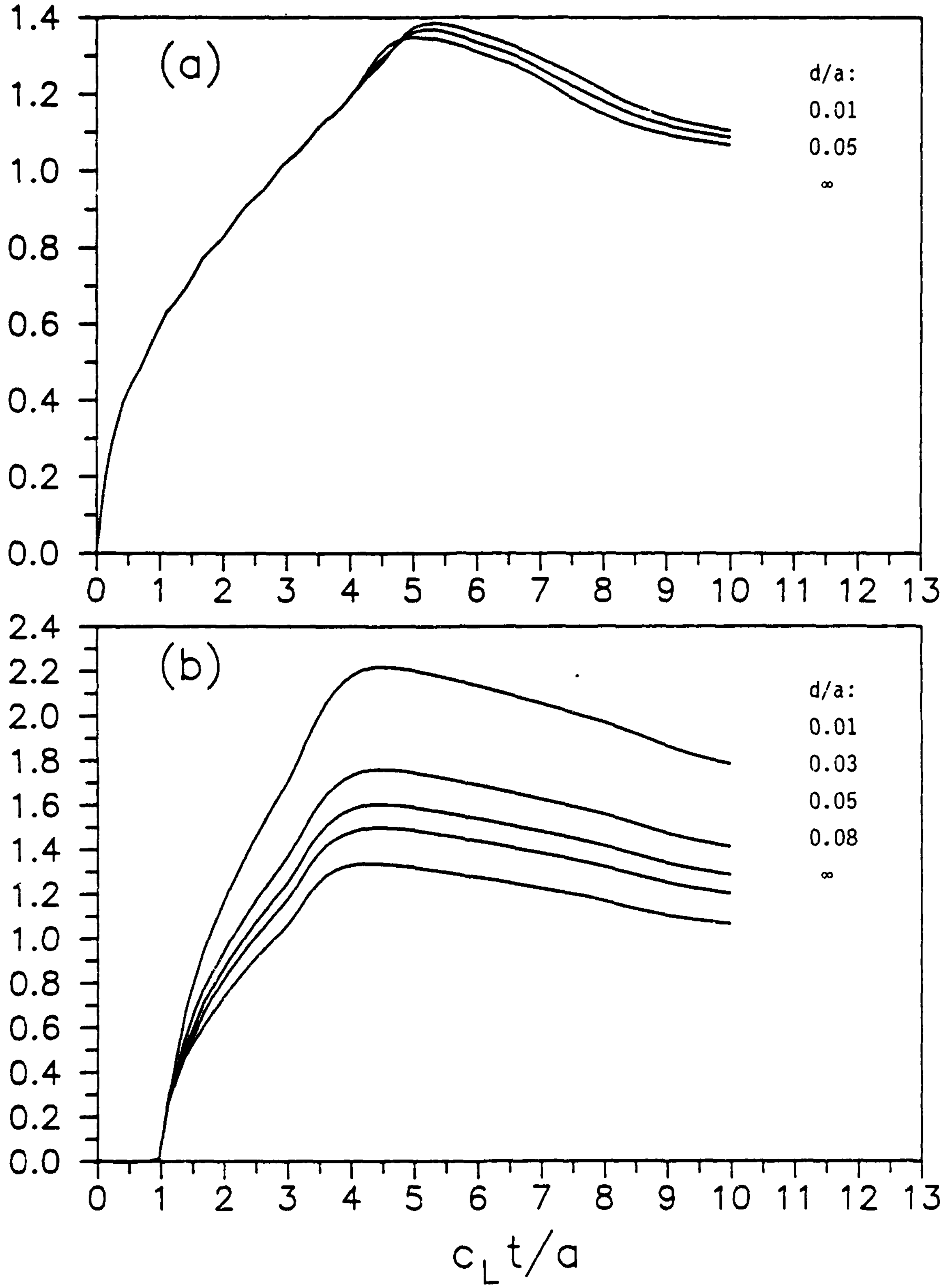

Fig. 4: Normalized stress intensity factors for various d/a, and for a plane L-wave incident under ϕ = 30°, b/a = 0.1; (a) $\overline{K}_I^-$; (b) $\overline{K}_I^+$.

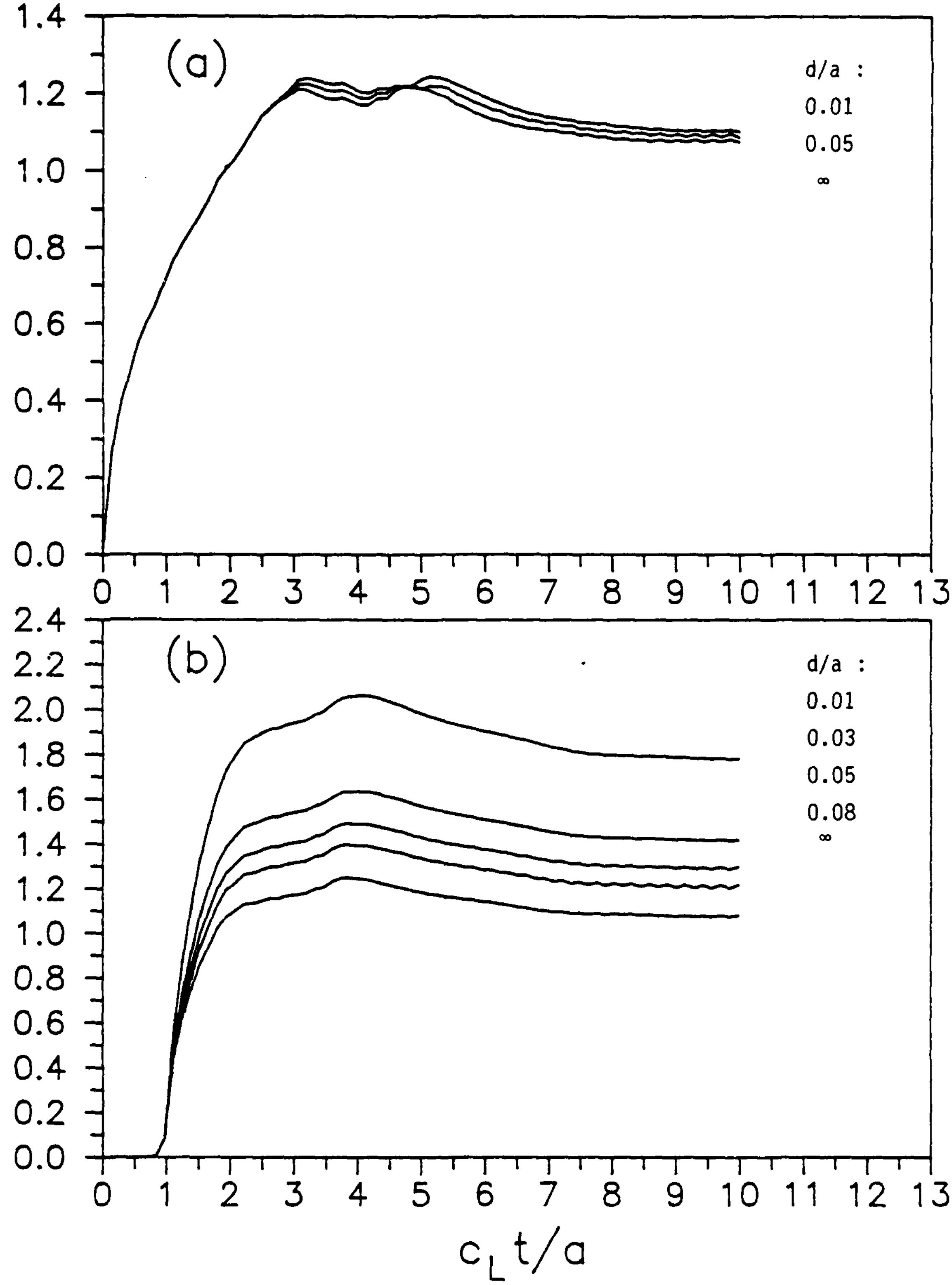

Fig. 5: Normalized stress intensity factors, for various d/a, and for a plane L-wave incident under $\phi = 30°$, $b/a = 0.1$; (a) $\overline{K}^{-}_{II}$; (b) $\overline{K}^{+}_{II}$.

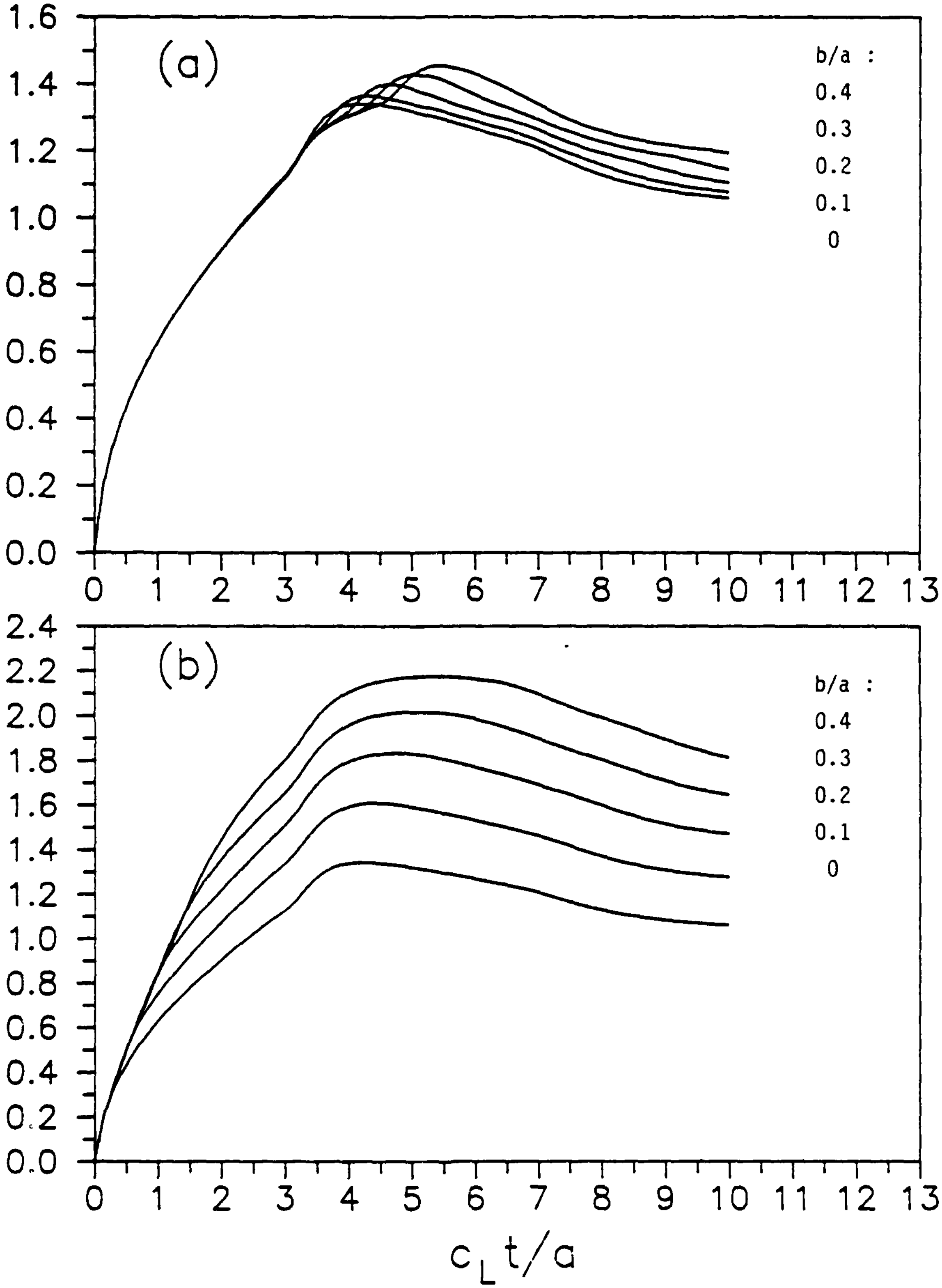

Fig. 6: Normalized stress intensity factors for various b/a, and for normal incidence of a plane L-wave, d/a = 0.05; (a) $\overline{K}_I^-$; (b) $\overline{K}_I^+$.

Unclassified

SECURITY CLASSIFICATION OF THIS PAGE (When Data Entered)

REPORT DOCUMENTATION PAGE		READ INSTRUCTIONS BEFORE COMPLETING FORM
1. REPORT NUMBER NU-SML-88-1	2. GOVT ACCESSION NO.	3. RECIPIENT'S CATALOG NUMBER
4. TITLE (and Subtitle) Time-Domain Boundary Element Analysis of Dynamic Near-Tip Fields for Impact-Loaded Collinear Cracks		5. TYPE OF REPORT & PERIOD COVERED Interim
		6. PERFORMING ORG. REPORT NUMBER
7. AUTHOR(s) Ch. Zhang and J. D. Achenbach		8. CONTRACT OR GRANT NUMBER(s) N00014-85-0401
9. PERFORMING ORGANIZATION NAME AND ADDRESS Northwestern University, Evanston, IL 60208		10. PROGRAM ELEMENT, PROJECT, TASK AREA & WORK UNIT NUMBERS
11. CONTROLLING OFFICE NAME AND ADDRESS Office of Naval Research Structural Mechanics Department Department of the Navy, Arlington, VA 22217		12. REPORT DATE February 1988
		13. NUMBER OF PAGES 32
14. MONITORING AGENCY NAME & ADDRESS(if different from Controlling Office)		15. SECURITY CLASS. (of this report) Unclassified
		15a. DECLASSIFICATION/DOWNGRADING SCHEDULE

16. DISTRIBUTION STATEMENT (of this Report)

Approved for public release; distribution unlimited

17. DISTRIBUTION STATEMENT (of the abstract entered in Block 20, if different from Report)

18. SUPPLEMENTARY NOTES

19. KEY WORDS (Continue on reverse side if necessary and identify by block number)

elastodynamic stress intensity factors
macrocrack
microcrack
time-domain boundary element method

20. ABSTRACT (Continue on reverse side if necessary and identify by block number)

A time- domain boundary integral equation method has been developed to calculate elastodynamic fields generated by the incidence of stress (or displacement) pulses on single cracks and systems of two collinear cracks. The system of boundary integral equations has been cast in a form which is amenable to solution by the boundary element method in conjunction with a time-stepping technique. Particular attention has been devoted to dynamic overshoots of the stress intensity factors. Elastodynamic stress intensity factors for pulse incidence on a single crack have been computed as functions of time, and they

DD FORM 1 JAN 73 1473 EDITION OF 1 NOV 65 IS OBSOLETE

Unclassified

SECURITY CLASSIFICATION OF THIS PAGE (When Data Entered)

have been compared with results of other authors. For collinear macrocrack-microcrack configurations the stress intensity factors at both tips of the macrocrack have been computed as functions of time for various values of the crack spacing and the relative size of the microcrack.

END
DATE
FILMED
6-1988
DTIC